ELSEVIER

Journal of Molecular Catalysis A: Chemical 98 (1995) 35–48

JOURNAL OF MOLECULAR CATALYSIS A: CHEMICAL

Effect of the synthesis conditions on the crystallinity and surface acidity of SAPO-11

M. Alfonzo [a], J. Goldwasser [a], C.M. López [a,*], F.J. Machado*[,a], M. Matjushin [a], B. Méndez [a], M.M. Ramírez de Agudelo [b]

[a] *Escuela de Química, Facultad de Ciencias, UCV, Apartado 47102, Caracas 1020-A, Venezuela*
[b] *INTEVEP, S.A, Apartado 76343, Caracas 1070-A, Venezuela*

Received 31 August 1994; accepted 11 January 1995

Abstract

A series of $AlPO_4$-11 molecular sieves with Si content ranging from zero to 0.24 Si molar fraction were crystallized from reaction gels prepared using different sources of Al and Si. It was found that the lower the crystallinity of the starting alumina the higher its reactivity and the higher the crystallinity and purity of the resulting molecular sieves. Factors affecting the initial pH of the departing gel strongly influence both the crystallinity and purity of the resulting solid. Thus, starting from the same source of alumina, it can be observed that the higher the pH within the acid region the higher the crystallinity and purity of the product. There seems to be an upper limit for the amount of Si incorporated in the $AlPO_4$-11 framework, above which isolated silica patches (silica domain) are formed and subsequently dislodged from the structure when calcination is carried out at 773 K, yielding α-quartz. At this limiting value the population of both Lewis and Brønsted acid sites passes through a maximum. Unreacted pseudoboehmite coexisting with SAPO-11, was transformed upon calcination at 773 K into γ-alumina. These species seem to act as Lewis centres which would interact with Brønsted sites to increase surface acidity.

Keywords: Acidity; Aluminophosphate; Crystallinity; NMR spectroscopy; SAPO-11; Synthesis

1. Introduction

Silicoaluminophosphate molecular sieves first reported by Lok et al. [1] have been shown to exhibit interesting catalytic properties for acid catalyzed hydrocarbon transformations. These microporous solids are prepared from reactive silicoaluminophosphate gels containing an organic amine as a template. SAPO-11 is a medium pore molecular sieve which has recently been used as acid catalyst for commercially attractive chemical reactions such as olefins skeletal isomerization and oligomerization [2]. This structure is usually prepared by hydrothermal treatment at 473 K of a starting gel containing pseudoboehmite as a source of aluminium, H_3PO_4 as a source of phosphorus, a source of silica and di-n-propylamine (DPA) as organic template.

The acidity and the catalytic properties will strongly depend on the Si content, sitting and ordering in the SAPO lattice. When silicon atoms are introduced in the framework of a hypothetical $AlPO_4$ structure at the phosphorus sites, potential Brønsted acidity is generated (mechanism SM2). Alternatively, the silicon substitution can result in the simultaneous replacement of a pair of Al + P

* Corresponding author. Fax. (+58-2)6931653/9797037.

SSDI 1381-1169(95)00004-6

atoms by two Si atoms (mechanism SM3). However, in the latter case the avoidance of Si–O–P bonds implies the combination of the mechanism SM2 together with the SM3. Several topological models have recently been advanced for the Si, Al and P distribution in the SAPO framework [3,4]. According to these proposals, the framework composition of such materials is not homogeneous and different compositional domains are thought to exist. In any case it seems to be clear that the resulting atomic distribution and, consequently, the acidity properties (the way silicon atoms are introduced) will depend on the synthesis procedure.

This work is aimed to examine the effect of the starting materials and the chemical composition of the departing gel over the properties of the resulting SAPO-11 molecular sieves.

2. Experimental

2.1. Synthesis

The following starting materials were used for the synthesis: pseudoboehmite (Catapal B from Vista Chemical Co.), pseudoboehmite (Disperal from Condea Chemie), gibbsite (from Interalumina); 40 wt% SiO_2 colloidal silica (Ludox AS 40 from Dupont), 99 wt% SiO_2 precipitated silica commercially designated as Agrosil 300 (from a local company called Venesil); 85% phosphoric acid (Aldrich); di-n-propylamine (DPA from Aldrich); di-i-propylamine (DIPA from Aldrich) and distilled water.

To prepare the synthesis gels the source of alumina was firstly added to a diluted phosphoric acid solution, then the amine and finally the source of silica were subsequently added, at room temperature under vigorous stirring until a homogeneous gel was obtained. The composition and some other characteristics of the resulting gels are given in Table 1. With the exception of the sample S-7 for which the stirring time was 3 h, all the remaining gels were agitated for 6 h before crystallization. Gels were then transferred into 60 ml Teflon lined stainless-steel autoclaves and heated at 473 K for 24 h (12 h for the sample S-10). The solid products recovered by centrifugation were copiously washed with distilled water and dried at 353 K overnight. To remove the amine the solids were statically calcined at 773 K for 15 h. The heating rate was about 5 K per minute and stops at 373 and 473 K for 1 h each were done before reaching the final calcination temperature.

Table 1
Results of the synthesis experiences. See experimental section for conditions

Sample	Gel molar composition	Starting materials	pH (b.c.)	pH (a.c.)	Result
A-0	Al_2O_3:P_2O_5:DPA:50H_2O	Catapal B; Ludox AS40	4.1	10.4	$AlPO_4$-11
S-1	Al_2O_3:P_2O_5:0.3SiO_2:0.5DPA:50H_2O		2.5	9.8	SAPO-11+T
S-2	Al_2O_3:P_2O_5:0.3SiO_2:DPA:50H_2O		3.9	10.9	SAPO-11
S-3	Al_2O_3:P_2O_5:0.6SiO_2:DPA:50H_2O		3.6	10.9	SAPO-11
S-4	Al_2O_3:P_2O_5:1.2SiO_2:DPA:50H_2O		3.9	7.7	SAPO-11
S-5	Al_2O_3:0.9P_2O_5:0.3SiO_2:DPA:50H_2O		5.8	9.6	SAPO-11
S-6	Al_2O_3:P_2O_5:0.3SiO_2:DIPA:50H_2O		3.3	7.4	SAPO-11
S-7	Al_2O_3:P_2O_5:0.3SiO_2:DPA:50H_2O		6.1	10.6	SAPO-11
S-8	Al_2O_3:P_2O_5:0.3SiO_2:DPA:50H_2O	Catapal B; Agrosil 300	3.0	8.4	SAPO-11+T,C,B
S-9	Al_2O_3:P_2O_5:0.3SiO_2:DPA:50H_2O	Disperal; Ludox AS40	3.0	8.2	SAPO-11+T
S-10	Al_2O_3:P_2O_5:0.3SiO_2:DPA:50H_2O [a]		3.0	11.0	T+SAPO-11
S-11	Al_2O_3:P_2O_5:0.3SiO_2:DPA:50H_2O	Gibbsite; Ludox AS40	2.5	6.3	T+G
S-12	Al_2O_3:P_2O_5:0.3SiO_2:4DPA:50H_2O	Gibbsite; Agrosil 300	5.2	7.0	T+C

(b.c.), (a.c.): before and after crystallization; T, C, B and G: Trydimite, Cristobalite, Berlinite and Gibbsite.
[a] 12 h crystallization.

2.2. Characterization

Al and P contents of the calcined solids were determined with the aid of an atomic emission spectrometer having a source of plasma inductively coupled. Si content was analyzed by atomic emission spectrometry. Samples were previously fused with lithium metaborate and dissolved in diluted nitric acid before the analyses. N_2-specific surface areas were obtained on a Micromeritics 2200 sorptometer at liquid nitrogen temperature. All the samples were pretreated at 623 K under vacuum overnight. X-ray diffractograms of the solid products before (as-prepared) and after calcination were recorded with a Philips diffractometer PW 1730 using Co-Kα radiation ($\lambda = 1.790255$ Å) operated at 30 kV, 20 mA and scanning speed of 2° 2θ/min. Diffraction lines between 8 and 25° 2θ were taking to determine the degree of crystallinity in the usual way. The sample S-2 with the higher intensity summation of the chosen lines was taking as to be 100% crystalline. Scanning electron micrographs were taken on a Hitachi S-500 microscope operated at 20 keV and 50 mA. The samples were Au-coated for 15 min on an Eiko Engineering instrument.

FTIR experiments were performed on a Perkin Elmer 1760-X spectrometer. Self supporting wafers of about 20 mg of sample previously calcined were placed into a Pyrex vacuum cell specially designed for gas and thermal 'in situ' treatments. First, the specimens were outgassed at 673 K under vacuum overnight. Afterwards, the temperature was dropped to 363 K and pyridine was admitted to the cell. Then, the excess pyridine was evacuated. All the spectra in the pyridine region were recorded after outgassing at 453 and 553 K. To study the mid-IR region, where structural T–O vibration occurs (below 1200 cm^{-1}), KBr-sample pellets were used and the spectra taken at room conditions.

^{27}Al, ^{31}P and ^{29}Si MAS NMR spectra were recorded in a Bruker AM 300 spectrometer under the following operation conditions for ^{27}Al, ^{31}P and ^{29}Si nucleus respectively: resonance frequency of 78.20, 121.49 and 59.63 MHz; repetition time of 1, 20 and 5 s; MAS frequency of 3900 in all cases; scan number of [800–2500], [40–200] and [8000–33000]. External references were $Al(H_2O)^{+3}$, 85 wt% H_3PO_4 and TMS. All the spectra were obtained by single-pulse excitation. For phosphorus high-power decoupling was applied.

3. Results and discussion

3.1. Synthesis

Synthesis experiences leading to different solid phases are given in Table 1. It can be observed that those reacting gels containing pseudoboehmite (Catapal B) as a source of alumina yielded the desired $AlPO_4$-11 structure. Replacing pseudoboehmite (Catapal B) by gibbsite resulted in a mixture of well-crystallized $AlPO_4$–tridymite (T) and unreacted gibbsite (G) (sample S-11). A different source of pseudoboehmite, commercially designated as Disperal, was also used as starting material. In this case the final product, regardless of the crystallization time, consisted of a mixture of SAPO-11 and $AlPO_4$–tridymite (T). The X-ray diffractograms of the resulting solids are given in Fig. 1.

The previous results can be explained in terms of the relative reactivity of the alumina employed, that is in turn associated to its relative crystallinity. X-ray diffractograms of the three different types of alumina used are shown in Fig. 2. From this figure gibbsite looks like the most ordered structure of them. A comparison of the X-ray diffractograms of the two pseudoboehmite materials indicates that Catapal B is the less crystalline one. The pH values of the reacting gels before crystallization shown in Table 2, reflect the amount of unreacted H_3PO_4 and consequently can also be taken as an index of the relative reactivity of the alumina source. Thus, by comparing the samples S-2, S-9 and S-11 prepared under the same conditions, it can be observed that the pH values decrease as the crystallinity of the alumina increases.

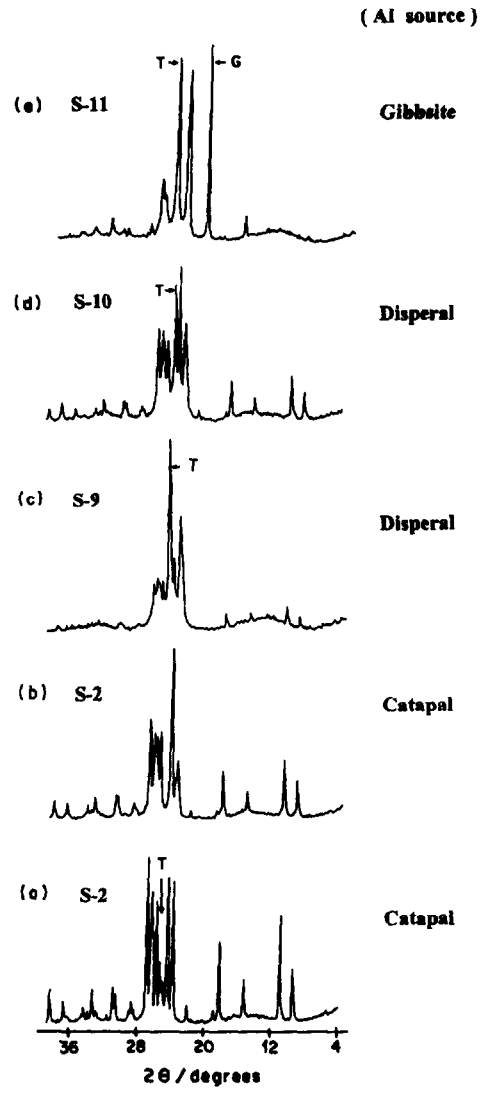

Fig. 1. X-ray diffraction patterns of the solid products obtained from three different sources of alumina. (T) $AlPO_4$–tridymite and (G) gibbsite.

The reactivity of the alumina will indeed affect the rate of nucleation and crystallization and therefore the resulting solid phase. It has already been established that dense phases are the initial products of the gel transformation [5]. Therefore, this is not surprising that the less reactive alumina, gibbsite, yielded tridymite as the major product (sample S-11). The less reactive pseudoboehmite, Disperal, gave a mixture of tridymite and SAPO-11 (sample S-9) and the more reactive pseudoboehmite, Catapal B, leaded to SAPO-11 as the only solid phase (sample S-2). These observations also suggest that $AlPO_4$–tridymite is the initial dense phase formed from this particular phase system.

In order to verify the latter hypothesis two forms of synthesis, leading to samples S-9 and S-10 of Table 1, were carried out. Thus, sample S-10 was prepared from the same reacting gel as the one used for the preparation of the sample S-9 but halving the time of crystallization (12 h). As can be observed from the X-ray diffractogram of this sample, shown in Fig. 1-c, the major phase of the resulting solid was tridymite slightly contaminated with SAPO-11. At 24 h of crystallization (sample S-9) the proportion of these two phases was reversed. It is noteworthy that the final pH value (after crystallization) of the S-10 preparation, leading to a dense phase as a major product, was 3 units higher than that observed for S-9. This clearly indicates the presence of a higher amount of free amine for the former, in agreement with its lower proportion of SAPO-11 molecular sieve.

Solid products having the desired $AlPO_4$-11 structure with a Si/(Al+P) ratio ranging from zero to 0.3 were successfully prepared from Catapal B as can be observed from Table 1 (samples A-0, S-2, S-3 and S-4). A sample of highly pure and crystalline SAPO-11 was also obtained from

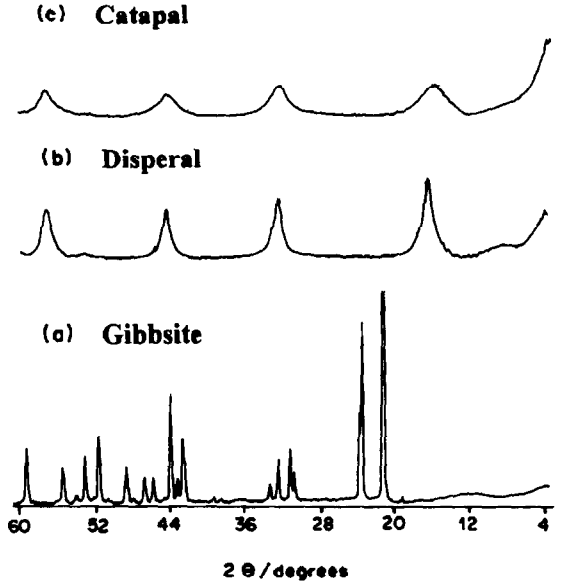

Fig. 2. X-ray diffractograms of the three sources of alumina employed in the synthesis.

a reacting gel having a P/Al ratio lower than unity (S-5). By contrast, in a previous work [6] both dense and amorphous phases were the only products obtained from the same source of alumina (Catapal B). In the latter case longer crystallization times and stirring were used during the crystallization period. On certain preparations the occurrence of small amounts of dense phases could not be avoided. In fact, a second preparation made under identical conditions as those used to synthesize the sample S-2 yielded, as can be observed from Fig. 1-a, SAPO-11 slightly contaminated with tridymite. The same phenomenon was observed for the sample S-7 for which the initial stirring time during the preparation of the reacting gel was halved (3 h). These unpredictable results indicate that the formation of dense phases depends to a certain extent on factors difficult to control during the synthesis procedure. Small temperature changes during the crystallization process (± 5 K), resulting from temperature controller limitation, might have accounted for the observed differences.

The sample S-1 for which the amount of DPA was halved was found to be slightly contaminated with $AlPO_4$–tridymite. In this case the low pH value of the resulting departing gel played a retarding role in the crystallization kinetic. When DIPA was used as a template in place of DPA, a solid mixture having SAPO-11 as the major crystalline phase was obtained (sample S-6). Minor unidentified components were also detected by XRD for this preparation. Similarly the sample S-8 prepared by using Agrosil 300 instead of Ludox AS40 as a source of silica showed a mixture of crystalline phases consisting of SAPO-11, $AlPO_4$–tridymite (T), $AlPO_4$–cristobalite (C) and berlinite (B). Again, the occurrence of dense phases is closely related to the pH of the departing gel. The corresponding X-ray diffractograms of these products are presented in Fig. 3.

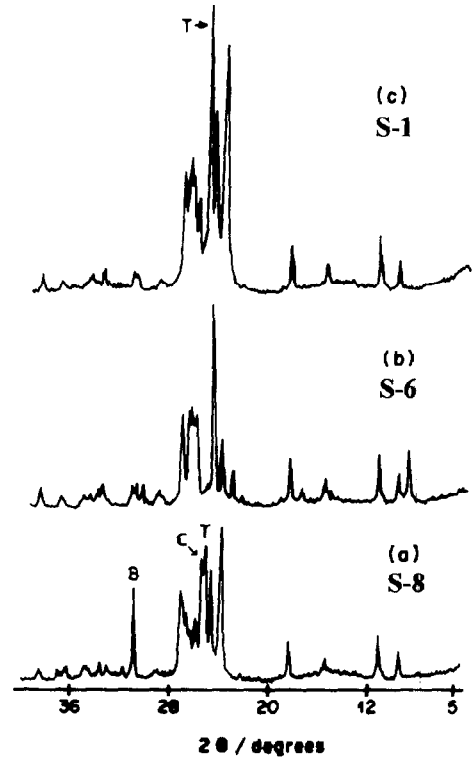

Fig. 3. X-ray identification of different solid phases resulting from changes in the synthesis procedures. (T) $AlPO_4$–tridymite; (B) $AlPO_4$–berlinite and (C) $AlPO_4$–cristobalite.

From the previous results it appears that both the sources of alumina and silica play an important

Table 2
Some characteristics of the synthetic samples

Sample	SSA (m^2/g)	% Crystallinity [a]		Molar composition formula TO_2	Unit cell parameters (Å)		
		b.c.	a.c.		*a*	*b*	*c*
A-0	167	70	98	$Al_{0.5}P_{0.5}O_2$	18.67	13.33	8.39
S-2	90	100	100	$Al_{0.48}P_{0.47}Si_{0.05}O_2$	18.76	13.42	8.43
S-3	163	73	42	$Al_{0.43}P_{0.43}Si_{0.14}O_2$	18.73	13.40	8.44
S-4	125	61	42	$Al_{0.38}P_{0.38}Si_{0.24}O_2$	18.45	13.33	8.38
S-7	126	66	72	$Al_{0.544}P_{0.386}Si_{0.071}O_2$	18.70	13.42	8.41

[a] b.c. = before calcination; a.c. = after calcination.

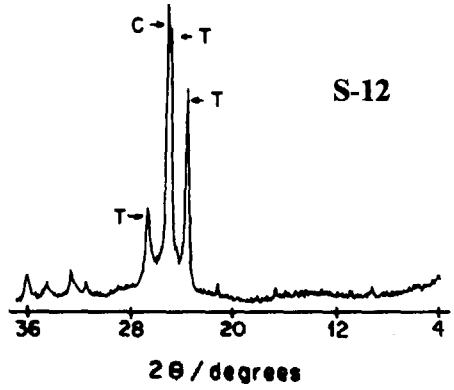

Fig. 4. X-ray diffractograms of the sample S-12 showing the different dense phases obtained. See text for details. (T) $AlPO_4$–tridymite and (C) $AlPO_4$–cristobalite.

role on the structure of the resulting solid. However, whereas the influence of the alumina is related to its degree of reactivity, in the case of silica the major factor seems to be associated with its basic character. Thus, Ludox AS40 being a colloidal silica solution stabilized with ammonium hydroxide to give a pH of about 10, gives rise to a departing gel with a higher pH value than that obtained from Agrosil 300. The interval of pH values previously reported for the synthesis of pure $AlPO_4$-based molecular sieves lies above 3.5 units [7].

In a separate experiment the two worst starting materials, this is to say: Agrosil 300 and gibbsite, were used as sources of Si and Al, respectively. The initial pH was adjusted to a value of 5.2, by increasing the proportion of DPA, to increase the rate of crystallization. The resulting solid (S-12) consisted of a mixture of dense phases $AlPO_4$–cristobalite and $AlPO_4$–tridymite, as shown in Fig. 4. Interestingly, by contrast with the preparation S-11, this time unreacted gibbsite was not observed. This result clearly indicates that the rate of crystallization was indeed increased by increasing the pH of the medium but not enough to obtain the desired SAPO-11 phase.

3.2. Characterization

Some characteristics of the products having the $AlPO_4$-11 structure are given in Table 2. The cell parameters of these materials, calculated before calcination, are in good agreement with those previously reported in the literature for a body-centred orthorhombic unit cell of $AlPO_4$-11-like structures [8].

After calcination at 773 K and partial rehydration at room conditions a significant change in the XRD patterns occurs, as illustrated in Fig. 5. This phenomenon, previously described in the literature [9], has been associated with a change in the crystal symmetry from a body-centred to a primitive unit cell as a result of water adsorption after calcination.

An attempt to index the XRD lines of the solids after the calcination–rehydration process was done. For this, the computing program PDP (Pow-

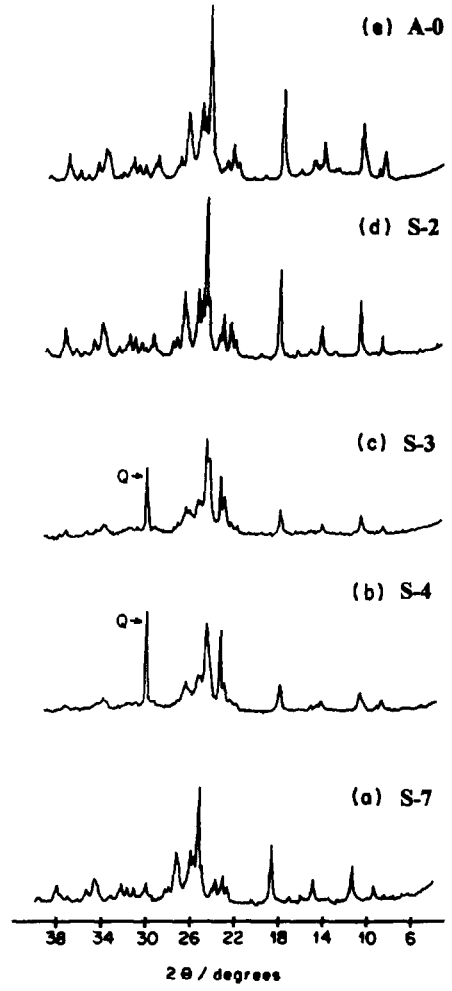

Fig. 5. X-ray diffractograms of the solid products quoted in Table 2 after calcination. (Q) α-quartz.

der Diffraction Package) [10] was applied to at least 13 of the most intense diffraction lines. To be able to index an orthorhombic system the above mentioned program requires the cell parameters values to be given. By taking the cell parameters reported by Tapp et al. [9] for a primitive orthorhombic unit cell of an $AlPO_4$-11, only those solids having a Si content between zero and 0.07 molar fraction were successfully indexed. Those solids with higher Si loading, failing to be indexed, additionally showed a well-defined XRD line at $d = 3.37$ Å (see Figs. 5-c and 5-b) corresponding to the 101 line of α-quartz. The intensity of this line increases as the Si content increases. Interestingly, this line is not present in the diffractograms of the uncalcined (as-prepared) solids.

The occurrence of α-quartz can be explained by assuming a situation by which structural patches of pure silica are formed within the framework of SAPO-11 as the Si content increases. In such a case, and as a result of the calcination treatment, these well-ordered silica patches are dislodged from the SAPO structure forming a denser α-quartz phase and causing a partial crystalline collapse of the remaining molecular sieve phase. A schematic representation of this proposal is given in Fig. 6. This diagram is based on that depicted by Martens et al. [3]. In the present case, however, a particularization has been made to fit our results. Thus, a domain of pure silica and another one of $AlPO_4$ joined together by a transition region consisting of a SAPO phase, are envisaged. To arrive at such a situation, the Si atoms should be incorporated within the hypothetical starting $AlPO_4$ structure, by a combination of SM2 and SM3 mechanisms in a similar way to the **3 + 2** model proposed by Dwyer et al. [4]. In this case the Si(4Al) environment, observed only when the SM2 mechanism occurs, is not to be expected. The ^{29}Si MAS NMR spectra of the uncalcined S-7 sample showed, as illustrated in Fig. 7-a, two well-differentiated Si environments. The first one related to the signal at about -112 ppm is associated to the Si(4Si) environment. The second one, less defined and having a maximum at around -97 ppm, is assigned to Si(nSi, $4-n$ Al) environments for $0 < n < 4$, where some Si atoms might be linked to terminal OH groups as has already been shown [11]. In the Fig. 7-b, the ^{29}Si MAS NMR spectrum of the calcined S-7 material, is presented. For this sample, the Si(nSi, $4-n$ Al) environments are apparently absent and an increase in the Si(4Si) signal is also observed. These changes might be ascribed to a sort of recrystallization of the defective Si–OH groups resulting in the generation of new dehydroxylated Si(4Si) environments. However, the high noise to signal ratio of this spectrum does not allow for a conclusive interpretation. The ^{29}Si MAS NMR spectra of both the as-prepared (Fig. 7-c) and the calcined (Fig. 7-d) specimens of the sample with the highest Si loading (S-4) showed a unique signal at -112 ppm. The sharpness of this line suggests the presence of Si(4Si) environments within ordered structures.

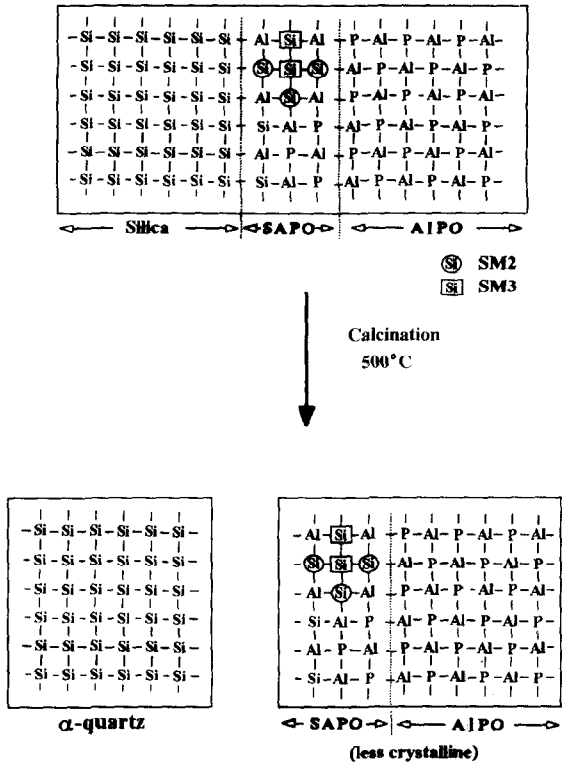

Fig. 6. Schematic representation of the generation of α-quartz from pure silica domain of SAPO-11. Si incorporation has been assumed to follow the **3 + 2** model of Ref. [4].

The relative proportion of the three different composition regions of Fig. 6 should depend on

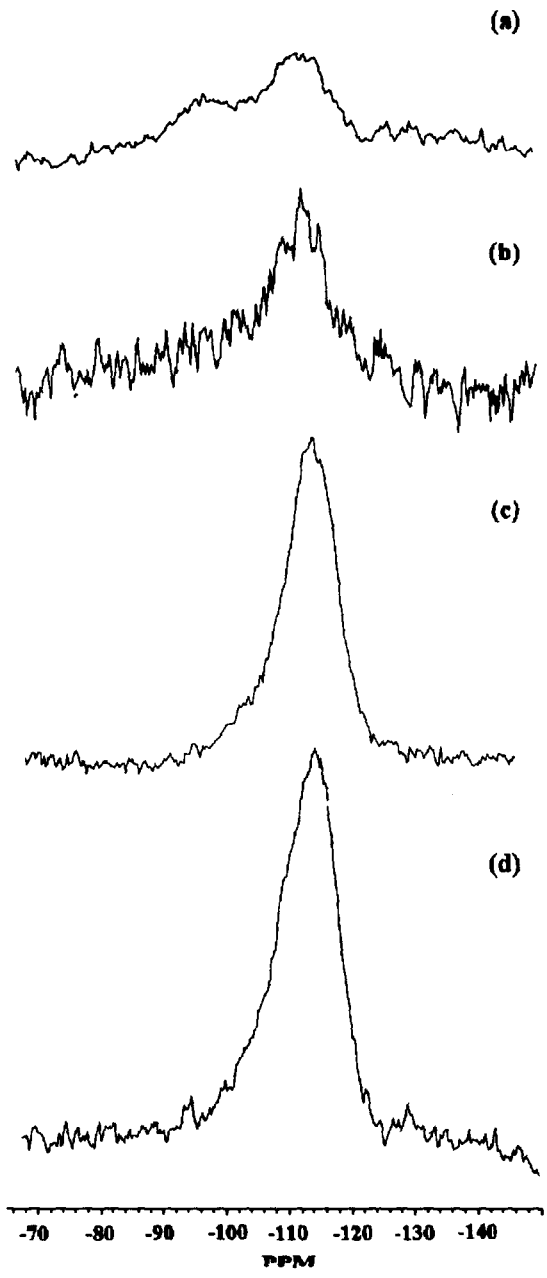

Fig. 7. ^{29}Si MAS NMR spectra of the solids (a) S-7 as-prepared; (b) calcined S-7; (c) S-4 as-prepared (d) calcined S-4.

the Si loading. Thus, at high Si levels the silica domain would be favoured and the feasibility of forming α-quartz would increase, as was actually observed (see Fig. 5). It should also be noted from Table 2 that after calcination the samples S-3 and S-4, having the highest Si content, yielded crystallinity values 40% lower than that taken as reference. All this seems to indicate that there is an upper limit for the amount of Si to be incorporated in the framework, above which drastic structural changes occur. To establish the exact position of this limit more data between the 0.07 and 0.14 Si molar fractions are needed.

The sample S-7 showed a crystallinity of about 35% lower than that corresponding to the sample S-2. For the former, as described in the Experimental section, the stirring time during the preparation of the reacting gel was halved. This fact might have affected the initial nucleation process giving rise to less ordered and smaller crystals. It is well known that the higher the rate of formation of the gel precursors during the preparation of solids such as alumina the higher the degree of crystal defects.

The SSA values of Table 2 lie within the range previously reported for this kind of solids [3]. Surprisingly, the sample S-2 with the higher degree of crystallinity showed the lowest adsorption capacity. Morphological analysis of this material, showed well-defined crystals with average sizes ranging between 2 and 5 microns, as can be observed from Fig. 8-a. By contrast, the samples S-3 and S-4, having higher SSA values, consist of esferulite-like aggregates of submicron crystals such as those shown in Fig. 8-b. These differences in crystal size and morphology cannot, however, fully explain the observed differences in their sorption capacities.

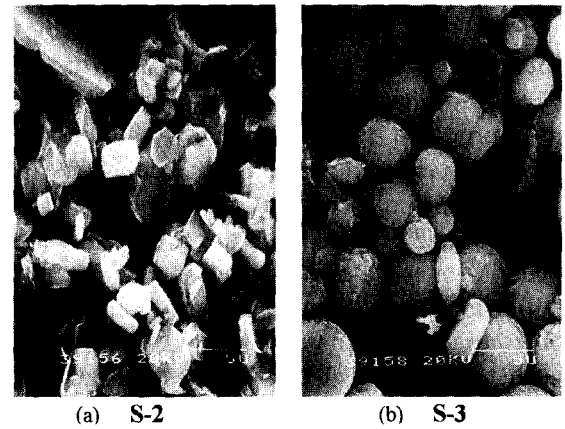

(a) **S-2** (b) **S-3**

Fig. 8. SEM photographs of samples (a) S-2 and (b) S-3.

The analysis of the average TO_2 formula, particularly for the solids with the highest silicon content (S-3 and S-4) would seem to indicate the occurrence of solely the SM3 mechanism. Since this way of Si incorporation is improbable, as has already been discussed, the compositional heterogeneity of this type of materials must be accepted. Thus, the model comprising an $AlPO_4$ region where Al/P = 1 and a silica domain linked together by a narrow SAPO zone, seems to match the results of the TO_2 analysis. The relatively high value of the Al/P ratio (1.41) observed for the sample S-7 suggests that there exists an excess of extra framework Al. In fact, the ^{27}Al MAS NMR spectrum of the as-synthesized solid shown in Fig. 9-a presented a signal at about 0 ppm, usually related to octahedral extra framework Al, in addition to the main one at around 40 ppm corresponding to tetrahedral framework Al in $AlPO_4$ environment. When an excess of pseudoboehmite was intentionally added to the sample S-7, the octahedral signal was increased, as can be observed from Fig. 9-b. Surprisingly, this signal completely disappeared in both cases after calcination at 773 K, as shown in Fig. 9-c. One should expect that after such thermal treatment pseudoboehmite were transformed into γ-alumina as predicted by the well-known alumina phase-transformation diagram. This transformation was indeed observed when a sample of pure Catapal-B was calcined under the same conditions. In the latter case, as illustrated in Fig. 9-d, two signals were observed, one at around 7 ppm corresponding to octahedral Al and another at around 60 ppm corresponding to tetrahedral Al. Such chemical shifts have been previously associated to γ-alumina [12]. Our first thinking was to associate the absence of the octahedral component, to a sort of transformation of the unreacted Catapal-B into low-symmetry polyaluminohydroxyl species, such as those thought to be formed in steamed ZSM-5, which were earlier associated with a shoulder at around the tetrahedral Al signal [13]. However, a physical mixture of separately calcined Catapal-B (20 wt%) and sample S-7 neither showed the octahedral signal, as can be observed from Fig. 9-e. The latter result led us to conclude that the octahedral component of the γ-alumina becomes undetectable by NMR in the presence of SAPO-11, even at concentrations as high as 20% by weight. When the proportion of calcined pseudoboehmite was increased to 40% by weight the octahedral signal begins to appear (spectrum not shown).

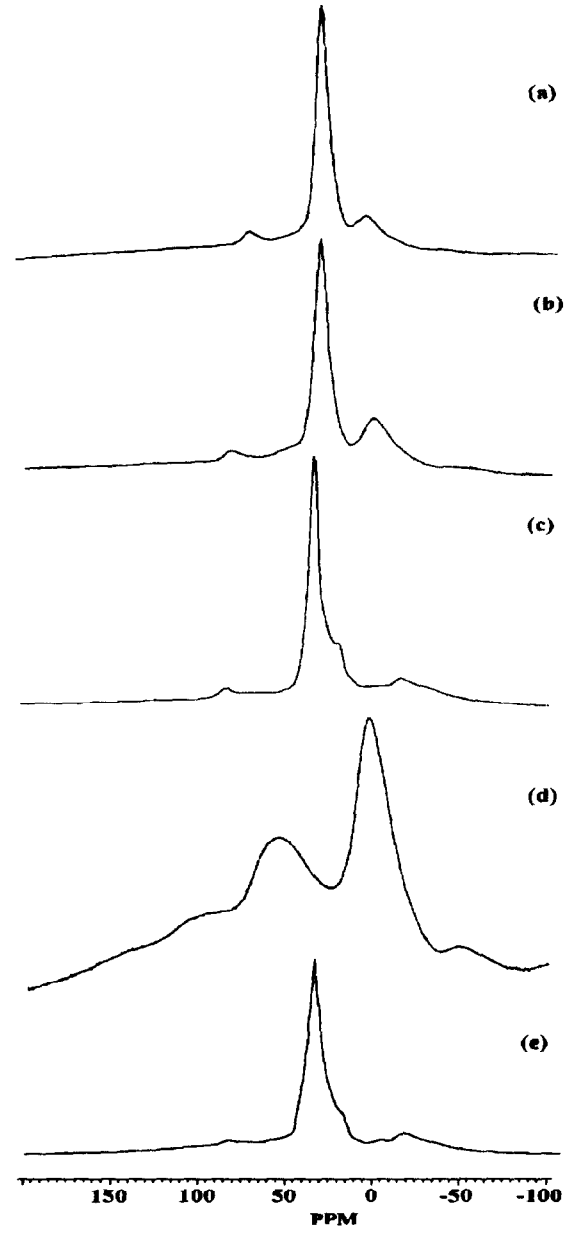

Fig. 9. ^{27}Al MAS NMR spectra of the solids (a) S-7 as-prepared; (b) S-7 + Catapal added; (c) calcined S-7 (d) calcined Catapal; (e) calcined S-7 + calcined Catapal (20 wt%)

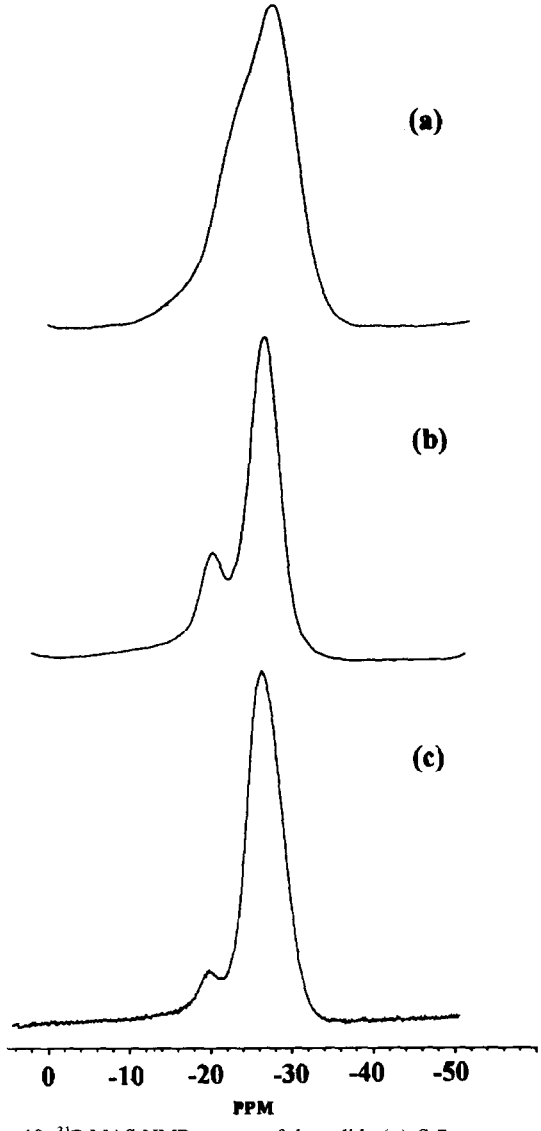

Fig. 10. ^{31}P MAS NMR spectra of the solids (a) S-7 as-prepared; (b) S-7 calcined and exposed to ambient (self hydrated) and (c) S-7 moisture-free stored (slightly hydrated).

The ^{31}P MAS NMR spectra of the sample S-7 as synthesized (a), calcined and exposed to ambient (b) and calcined and kept in a desiccator (c), are shown in Fig. 10. The observed behaviour agrees very well with previous findings [9,14]. That is to say, after calcination and self hydration (Fig. 10.b) two distinct peaks are clearly observed indicating the occurrence of at least two different non equivalent crystallographic sites for the tetrahedral P atoms. The chemical shift of these sites seems to be associated to their interaction with water molecules. What is important to note in the present case is the strong affinity with water shown by this structure. Thus, one of the calcined materials was stored moisture-free inside a desiccator. Then, it was moved into a glove-box and kept under dry anaerobic conditions. Finally, it was packed into a rotor cap, specially designed for such a purpose [15]. However, in spite of these precautions, even the short time spent moving the sample from the desiccator to the dry box was enough as to cause partial rehydration leading to the crystallographic differentiation (see Fig. 10.c).

FTIR spectra after pyridine adsorption at 363 K and desorption at both 453 and 553 K, of the solids prepared from reacting gels having different proportions of Si, are presented in Fig. 11. All the samples showed both Lewis and Brønsted sites interacting with pyridine after outgassing at 453 K. The samples S-2 and S-7, having the lowest Si content, showed the highest proportion of both kinds of sites. After outgassing at 553 K, both the Lewis and Brønsted bands almost completely disappear for samples S-3 and S-4 but still significantly remain for the samples with the lowest Si loading.

By observing the atomic distribution of Fig. 6 clearly Brønsted acidity must be associated with the SAPO-phase transition region. By adopting the stoichiometry of the **3+2** model of Ref. [4] for this boundary domain, it can be deduced that the substitution of four P atoms and one Al atom by five Si atoms is required to obtain the smallest silicon domain via the SM2+SM3 mechanism. The resulting local composition can then be expressed by the following formula in which protons have been included as charge-compensating cations:

$$H_{0.6x}[Al_{(0.5-0.2x)}P_{(0.5-0.8x)}Si_x]O_2 \qquad (I)$$

The equivalent expression for the local composition resulting from the SM2 mechanism would be:

$$H_x[Al_{0.5}P_{(0.5-x)}Si_x]O_2 \qquad (II)$$

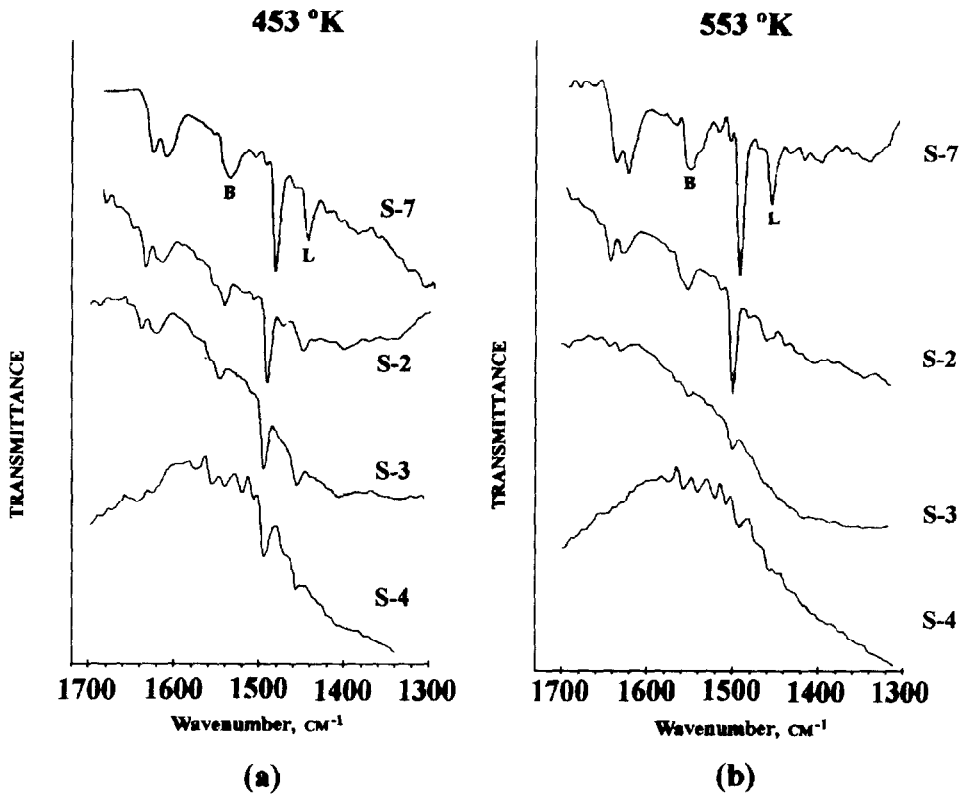

Fig. 11. FTIR spectra of the pyridine–SAPO-11 interaction after outgassing at (a) 453 K and (b) 553 K.

From the previous formulas the partial charge on the hydrogen atoms (ZH), an accepted index of the acid strength, can be calculated by applying the Sanderson electronegativity equalization principle and the resulting mathematical expressions as proposed by Mortier [16]. The results of such calculations are given in Table 3 for three different Si molar fractions and the two local compositions (formulas I and II) derived from the combined SM2 + SM3 and SM2 mechanisms respectively. Additionally, the data for three different zeolites of known acid strength, namely HY, H-Mordenite and H-ZSM-5, are also given for comparison.

Table 3
Partial charge on hydrogen atoms (ZH) derived from the Sanderson intermediate electronegativity (Sint) for several local SAPO compositions calculated from SM2 and combined SM2 + SM3 mechanisms (some protonic zeolites are included for comparison)

X	SM2			SM2 + SM3		
	[H]	Sint	ZH	[H]	Sint	ZH
0.01	0.01	4.21	0.168	0.006	4.21	0.169
0.10	0.10	4.16	0.157	0.060	4.18	0.163
0.24	0.24	4.07	0.134	0.144	4.14	0.152
HY (Si/Al = 2.5)	–	4.10	0.140	–	–	–
H-MOR (Si/Al = 5)	–	4.16	0.155	–	–	–
H-ZSM-5 (Si/Al = 31)	–	4.19	0.163	–	–	–

From this table it can be observed that at low Si loading, the partial charge resulting from both mechanisms is almost identical and slightly higher than the one corresponding to the proton form of a ZSM-5 zeolite having a Si/Al ratio of 31, widely recognized as possessing strong acid sites. In a recent paper [17] it was already suggested that Si(nAl) environments with $n < 4$, at the borders of the Si islands in SAPO-37, might create strong acid sites. As the Si content is increased ZH decreases and the differences between both mechanisms become evident. The acid strength of the structures resulting from the combined mechanism is higher than the one obtained by the SM2 mechanism. In both cases the proton concentration increases with the Si content but whereas the

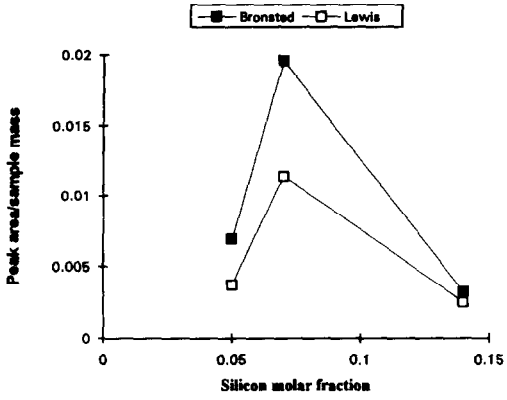

Fig. 12. Acid site populations after outgassing at 553 K as a function of the Si fraction

ratio [H]/[Si] is the unity for the SAPO resulting from the SM2 mechanism, this value drops to 0.6 for the combined one.

On the basis of the previous observations it is now possible to explain the observed higher acid strength of the samples with the lowest Si content. Moreover, by plotting the proton concentration as a function of the Si fraction it is expected to observe a decrease in the regression coefficient of the linear regression when switching from an SM2 mechanism ([H]/[Si] = 1) to an SM2 + SM3 mechanism ([H]/[Si] = 0.6). This behaviour was observed by Dwyer et al. [4] for SAPO-37 when the Si molar fraction reached 0.1. The lack of sufficient data, the generation of α-quartz with the corresponding loss of crystallinity and the contamination with alumina of some of the samples studied in the present work, prevented us from obtaining a better picture of the actual situation.

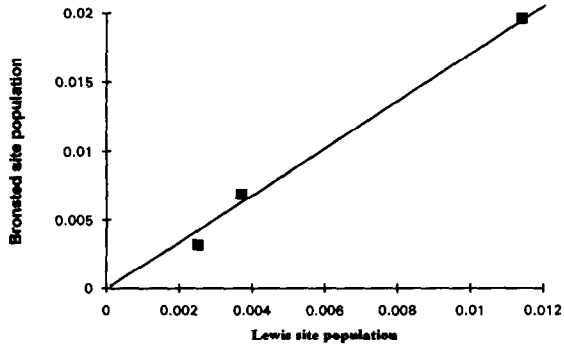

Fig. 13. Correlation between Brønsted and Lewis site population after outgassing at 553 K.

The previous analysis, based on the simple electronegativity model, can also rationalize the observed high performance of SAPO-11 in several acid-catalyzed reactions in spite of its low acid site density. Thus, as predicted by Martens et al. [3], the acid sites at the boundary transition region seem to be strong enough to exhibit high turnover numbers.

The highest acid character of the sample S-7 can also be due to the presence of extra framework γ-alumina. As known, this variety of alumina contains Lewis acid centres that can interact with structural Brønsted groups to generate sites of enhanced acidity. Aluminium species external to the lattice have been largely linked to Lewis and superacid sites in zeolites [18,19]. Indeed, for this sample the IR bands associated with both Lewis and Brønsted acid sites remained unaffected, showing better definition and higher intensities than those shown by the rest of the samples studied, even after outgassing at 553 K (see Fig. 11).

By plotting the concentration of both Brønsted and Lewis sites (peak area/sample mass) after outgassing at 553 K, as a function of the Si fraction, the correlation shown in Fig. 12 was found. Again, a maximum at 0.07 Si molar fraction, corresponding to the sample S-7, was observed. Furthermore, when plotting the Brønsted site population as a function of the Lewis site population, a linear correlation was obtained as shown in Fig. 13. This simultaneous increment of both types of acid sites is in line with the idea of a synergism between them. In the work by Su and Barthomeuf [17] it was suggested that the increase in acid strength, observed in SAPO-37 upon heating, might be related to an interaction between protons and Lewis acid sites.

The influence of the method of gelation on the resulting surface acidity cannot be neglected. The lowest gelation time used in the preparation of sample S-7 might have caused structural defects generating additional acid sites. Thus, surface acidity in $AlPO_4$-structures has been associated with structural defects leading to P–OH, Al–OH and Si–OH entities [20].

Mid-infrared spectra of the sample S-2 as-prepared and calcined as well as the one corresponding to the sample S-12 of Table 1 (tridymite + cristobalite) are presented in Fig. 14. In all cases the three main vibrations at around 1100, 700 and 500 cm^{-1} related to the asymmetric stretching, symmetric stretching and the bending of the structural T–O bonds are observed. A unique well-defined band at around 550 cm^{-1} is also present in the as-synthesized SAPO-11 (sample S-2). This band has been previously associated in zeolites to a fundamental T–O bending mode [21]. However, the absolute absence of this band in both the calcined–rehydrated material and the dense phase S-12, leads us to consider an association of this band with a sort of interaction between the organic base and the framework T-atoms. A similar behaviour has been previously observed in our laboratories on several materials having the $AlPO_4$-5 structure [22]. Furthermore, after the calcination–rehydration process a well-defined band was developed in the asymmetric stretching region and several new bands were observed in the symmetric stretching region (see Fig. 14-b).

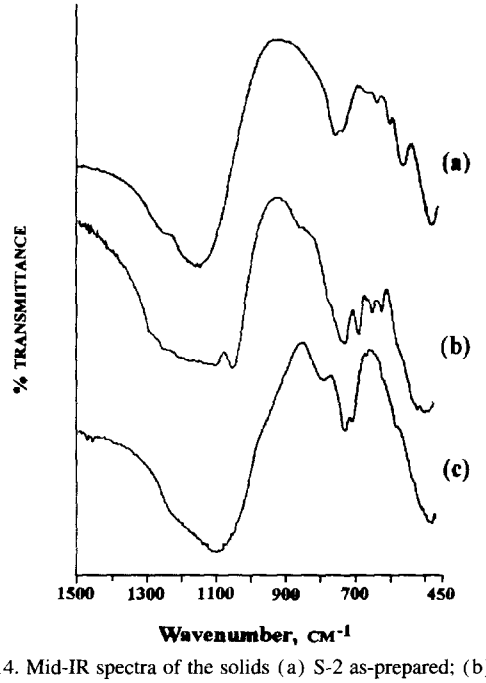

Fig. 14. Mid-IR spectra of the solids (a) S-2 as-prepared; (b) S-2 after calcination and (c) S-12 as-prepared.

4. Conclusions

Dense phases such $AlPO_4$–tridymite are first formed during the synthesis of SAPO-11. Therefore, all those factors leading to an increase of the crystallization rate will minimize the occurrence of such undesirable contaminants. Thus, less crystalline alumina structures are more reactive and the resulting molecular sieves more crystalline and less contaminated. Similarly, an increase in the pH values of the departing gel within the acid region lead to better materials.

When the Si content exceeds the value of 0.07 Si molar fraction not only a decrease in acidity occurs but also significant structural changes are observed. Silica patches are proposed to be formed within the structure of SAPO-11 as the Si content increases. These entities of pure silica would be dislodged from the framework, as a result of the calcination treatment, yielding a new phase of α-quartz and a less crystalline molecular sieve.

A model for the ordering of the T atoms in the SAPO-11 framework involving two well-differentiated $AlPO_4$ and silica domains linked through a SAPO-phase transition region was advanced. This model finds support on the combined SM2 + SM3 mechanism of Si incorporation, designated **3 + 2** in the recent literature [4]. The model can explain not only the structural changes observed but also the Brønsted acidity properties of this type of material. The occurrence of Si-rich domains in SAPO-*n* molecular sieves has also been confirmed in a recent report [23].

Unreacted extra framework pseudoboehmite is transformed under calcination into extralattice γ-alumina. A synergism between the Lewis centres of the alumina and the structural Brønsted sites, to yield a solid with an enhanced acid strength, was evidenced.

Acknowledgements

This work was supported by CONICIT project RPI-10001 and CDCH-UCV project 03-12-2324/90.

References

[1] B.M. Lok, C.A. Messina, R.L. Patton, R.T. Gajek, T.R. Cannan and E. Flanigen, US Pat. 4,440,871 (1984).
[2] J.A. Rabo, R.J. Pellet, P.K. Coughlin and E. Shamshoum, Stud. Surf. Sci. Catal., 46 (1989) 1.
[3] J. Martens, P. Grobet and P. Jacobs, J. Catal., 126 (1990) 299.
[4] M. Makarova, A. Ojo, K. Al-Ghefaili and J. Dwyer, Procc. IX Int. Zeolite Conf., Vol. II, 1992, p. 259.
[5] N. Tapp, N. Milestone and D. Bibby, Stud. Surf. Sci. Catal., 37 (1988) 393.
[6] M. Mertens, J. Martens, P. Grobet and P. Jacobs, NATO ASI SERIES. Series B: Physics, 221 (1990) 1.
[7] X. Ren, S. Komarneni and D. Roy, Zeolites, 11 (1991) 142.
[8] P.J. Barrie, M. Smith and J. Klinowski, Chem. Phys. Lett., 180 (1991) 6.
[9] N. Tapp, N. Milestone, M. Bowden and R. Meinhold, Zeolites, 10 (1990) 105.
[10] M. Calligaris, Powder Diffraction Package, version 1.1, Dipartimento di Scienze Chimiche, Universita di Trieste, Italy, 1990.
[11] P. Bodart, J.B. Nagy, G. Debras, Z. Gabelica and P. Jacobs, J. Phys. Chem., 90 (1986) 5183
[12] J. Sanz, J. Campelo and J. Marinas, J. Catal., 130 (1991) 642.
[13] A.G. Ashton, S. Batmanian, D.M. Clark, J. Dwyer, F.R. Fitch, A. Hinchcliffe and F.J. Machado, Stud. Surf. Sci. Catal., 20 (1985) 101.
[14] M. Peeters, J. de Haan, L. Van de Ven and J. Van Hoof, J. Phys. Chem., 97 (1993) 5363.
[15] L. Merwin, A. Sebald, Y. Esndel and R. Harris, J. Magn. Reson., 84 (1979) 367.
[16] W.J. Mortier, J. Catal., 55 (1978) 138.
[17] B. L Su and D. Barthomeuf, J. Catal., 139 (1993) 84.
[18] P. Jacobs and H.K. Beyer, J. Phys. Chem., 83 (1979) 1174.
[19] C. Mirodatos and D. Barthomeuf, J.Chem. Soc., Chem. Commun., (1981) 29.
[20] M. Burgers and H. van Bekkum, Stud. Surf. Sci. Catal., 78 (1993) 567.
[21] E. Flanigen, in J. Rabo (Ed.), Zeolite Chemistry and Catalysis, ACS Monograph 171, 1976, Chap. 2, p. 80.
[22] C. López, C. Urbina, D. Maspero, F. Machado and J. Perez-Pariente, Proc. XIII Iber. Symp. Catal., Vol. 2, 1992, p. 1035.
[23] R. Borade, A. Clearfield, J. Mol. Catal., 88 (1994) 249.